


# Simultaneous improvement of power density and durability of sulfonated poly(ether ether ketone) membrane by embedding CeO<sub>2</sub>-ATiO<sub>2</sub>: A comprehensive study in low humidity proton exchange membrane fuel cells

Hariprasad Ranganathan<sup>1,2</sup>  | Mohanraj Vinothkannan<sup>3,4</sup>  | Ae Rhan Kim<sup>1,5</sup>  |  
Vijayapradeep Subramanian<sup>1</sup> | Min-Suk Oh<sup>1,6</sup> | Dong Jin Yoo<sup>1,3,5</sup> 

<sup>1</sup>Department of Energy Storage/Conversion Engineering of Graduate School (BK21 FOUR), Hydrogen and Fuel Cell Research Center, Jeonbuk National University, Jeonju, Republic of Korea

<sup>2</sup>Institut National de la Recherche Scientifique-Énergie Matériaux et Télécommunications, Varennes, Quebec, Canada

<sup>3</sup>R&D Education Center for Whole Life Cycle R&D of Fuel Cell Systems, Jeonbuk National University, Jeonju, Republic of Korea

<sup>4</sup>Department of Energy Science and Engineering Research Center, Daegu Gyeongbuk Institute of Science and Technology (DGIST), Daegu, Republic of Korea

<sup>5</sup>Department of Life Science, Jeonbuk National University, Jeonju, Republic of Korea

<sup>6</sup>Division of Advanced Materials Engineering and Research Center for Advanced Materials Development, Jeonbuk National University, Jeonju, Republic of Korea

## Correspondence

Ae Rhan Kim and Dong Jin Yoo,  
Department of Energy Storage/  
Conversion Engineering of Graduate  
School (BK21 FOUR), Hydrogen and Fuel  
Cell Research Center, Jeonbuk National  
University, Jeonju, Republic of Korea.  
Email: [kimaerhan@jbnu.ac.kr](mailto:kimaerhan@jbnu.ac.kr) (A. R. K.)  
and [djyoo@jbnu.ac.kr](mailto:djyoo@jbnu.ac.kr) (D. J. Y.)

## Funding information

Korea Institute of Energy Technology  
Evaluation and Planning, Grant/Award  
Number: 2021400000040; National  
Research Foundation of Korea, Grant/  
Award Numbers: 2020R1A2B5B01001458,  
2021R111A1A01050905

## Summary

Herein, we describe the incorporation of cerium oxide-coated amine-functionalized titania nanorods (CeO<sub>2</sub>-ATiO<sub>2</sub>) as a bifunctional nanofiller in sulfonated poly(ether ether ketone) (SPEEK) as a cost-effective and high-performance proton exchange membrane (PEM) for PEM fuel cells (PEMFCs). Facile and effective functionalization of TiO<sub>2</sub> was performed using amine-containing organic moieties, followed by coating the ATiO<sub>2</sub> nanorods with CeO<sub>2</sub>. A simple solution casting method was employed to incorporate CeO<sub>2</sub>-ATiO<sub>2</sub> into the SPEEK matrix with various weight ratio of 0.5%, 1%, 2%, 4%, or 6%. The successful incorporation of prepared nanofiller in the SPEEK membrane matrix was confirmed by structural and morphological studies such as Fourier transform infrared, X-ray diffractometer, scanning electron microscopy, and atomic force microscope of the SPEEK/CeO<sub>2</sub>-ATiO<sub>2</sub> composite membranes. The presence of ATiO<sub>2</sub> improved proton conductivity while CeO<sub>2</sub> alleviated the chemical degradation of the membrane by scavenging free radicals. The proton conductivity of an SPEEK/CeO<sub>2</sub>-ATiO<sub>2</sub> (2 wt%) nanocomposite membrane at 60°C under 20% relative humidity (RH) was 17.06 mS cm<sup>-1</sup> whereas that of a bare SPEEK membrane under the same conditions was only 4.53 mS cm<sup>-1</sup>. PEMFCs containing SPEEK/CeO<sub>2</sub>-ATiO<sub>2</sub> (2 wt%) nanocomposite membrane attained a maximum power density of 117 mW cm<sup>-2</sup> at a load current density of 371 mA/cm<sup>2</sup> at 60°C under 100% RH. In contrast, a PEMFC containing the bare SPEEK membrane delivered a

power density of  $91 \text{ mW cm}^{-2}$  at a load current of  $253 \text{ mA cm}^{-2}$ . A single cell open circuit voltage (OCV) test to examine the durability of membranes revealed that a PEMFC with an SPEEK/CeO<sub>2</sub>-ATiO<sub>2</sub> (2 wt%) membrane showed excellent stability with an OCV decay of  $0.925 \text{ mV h}^{-1}$  at  $60^\circ\text{C}$  under 30% RH, whereas that of a PEMFC with a bare SPEEK membrane was  $3.437 \text{ mV h}^{-1}$  under identical conditions. Based on the abovementioned results, it is found that the SPEEK/CeO<sub>2</sub>-ATiO<sub>2</sub> nanocomposite membranes overcome the durability issues of pristine SPEEK membranes and show enhanced electrochemical performance under a harsh PEMFC environment.

### Highlights

- CeO<sub>2</sub>-ATiO<sub>2</sub> was utilized as a bifunctional filler to fabricate composite membrane.
- Integration of CeO<sub>2</sub>-ATiO<sub>2</sub> improved the proton conductivity of sulfonated poly(ether ether ketone) (SPEEK) under low relative humidity.
- Addition of CeO<sub>2</sub>-ATiO<sub>2</sub> to SPEEK resulted in improved physiochemical and thermomechanical properties.
- Optimized SPEEK/CeO<sub>2</sub>-ATiO<sub>2</sub> (2 wt%) exhibited improved proton exchange membrane fuel cell performance while retaining excellent durability compared to pristine SPEEK.

### KEYWORDS

durability, hybrid membranes, PEMFC, power density, radical scavenger

## 1 | INTRODUCTION

Proton exchange membrane fuel cells (PEMFCs) are one of the next-generation green energy sources for stationary and transport applications due to their environmental friendliness, extraordinary energy density, industrial adaptability, and transient response times.<sup>1</sup> In particular, progressive growth and modernization of automobiles and portable electronics have increased demand for low-cost PEMFCs.<sup>2,3</sup> However, the long-term durability of state-of-the-art PEMFCs still needs to be fully recognized to meet the large-scale requirements and implementation of the technology. Also, the high installing cost of PEMFC components, including the membrane electrode assembly (MEA), current collectors, and graphitic plates, is hindering the wide commercialization.<sup>4,5</sup> In a typical PEMFC, the MEA plays a crucial part in the overall performance outputs and the total cost. An MEA consists of three elements: a proton exchange membrane (PEM), two gas diffusion layers (GDLs), and catalyst layers (CLs).<sup>6-8</sup> The GDLs distribute the fuel or reactants into the active area, where the CL is coated in anode and cathode sides to improve the reaction kinetics of hydrogen oxidation reaction and oxygen reduction reaction (ORR), respectively. Meanwhile, the

PEM transfers protons from the anode to the cathode while preventing contact between hydrogen and oxygen gases. In general, an external humidifier is used to humidify the membrane for the rapid proton transfer, which consumes 20% of generated power from PEMFCs.<sup>9,10</sup> Hence, the development of a membrane that can function under low relative humidity (RH) or dry conditions can alleviate the need for an external humidifier. Also, under fully hydrated conditions, the accumulation of excess water on the cathode side prevents oxygen molecules from reaching the catalyst active area, which can be avoided under low RH operations.<sup>11,12</sup> Therefore, a membrane that can operate under anhydrous or low RH PEMFC conditions is of the great research interests.

DuPont's Nafion is probably the most widely used PEM in PEMFCs because of its good proton conductivity and chemical and thermal stability.<sup>12-14</sup> However, the Nafion's proton conductivity is strongly dependent on its humidification, and the membrane is expensive costing 17% of the total cost of a PEMFC system according to the US Department of Energy report in 2017.<sup>15</sup> Studies on cost-effective hydrocarbon membranes such as sulfonated poly(ether ether ketone) (SPEEK) membranes have demonstrated that these membranes can provide reasonable

PEMFC performance compared to Nafion.<sup>16–18</sup> The SPEEK membranes are derived from well-known semi-crystalline thermoplastic PEEKs that have high chemical resistance and good thermomechanical properties.<sup>19</sup> However, similar to Nafion, the proton conductivity of SPEEK membranes is strongly dependent on humidified water content. So, the SPEEK membranes have to be prepared with a high degree of sulfonation (DS) to achieve maximum electrochemical performance. On the other hand, the high DS (above 60%) causes the SPEEK matrix to absorb larger content of water under fully humidified conditions, which can trigger the matrix to swell in turn decreases the mechanical integrity and chemical stability of the membrane.<sup>20,21</sup> These limitations of SPEEK membranes can be avoided if PEMFCs are operated under low RH. Nevertheless, only fewer studies have been focused on the performance of SPEEK membranes in PEMFCs operating under a low humidity environment. Besides, the chemical and mechanical integrities of SPEEK membranes can be easily suppressed by the attack of free radicals which are rapidly generated under anhydrous or low RH PEMFC conditions.<sup>22–24</sup> Electrochemical performance, thermomechanical, and chemical stability of SPEEK membranes used in a low RH PEMFC environment can potentially be enhanced by improving the ability of the membranes to conduct protons in the absence of humidified water molecules and to withstand free radical attack. The former can be accomplished by incorporating hygroscopic nanofillers (SiO<sub>2</sub>, Sulfonated carbon nanotubes, Sulfonated graphene oxide, and ZrO<sub>2</sub>) for long-term retention of water molecules<sup>24–27</sup> or by dispersing functionalized nanoparticles (amines, phosphoric acid, and imidazole) containing self-humidified functional moieties into the SPEEK matrix for water-free proton conduction.<sup>27–30</sup> The latter can be achieved by reinforcing bare SPEEK membranes with free radical scavengers such as CeO<sub>2</sub> or MgO<sub>2</sub>. For instance, Salarizadeh et al incorporated amine-functionalized titania (NH<sub>2</sub>-TiO<sub>2</sub>) nanoparticles into SPEEK membranes and demonstrated that the functionalized ATiO<sub>2</sub> offered an additional hopping pathway for conduction of protons in addition to increasing overall PEMFC output.<sup>31</sup> Parnian et al prepared SPEEK-ceria (CeO<sub>2</sub>) nanocomposite membranes for PEMFCs that exhibited long-term durability due to the presence of radical scavenging CeO<sub>2</sub> nanoparticles.<sup>32</sup> However, SPEEK membranes with both enhanced electrochemical output and chemical sustainability under anhydrous or low RH PEMFC operations have yet to be reported. Accordingly, we synthesized a bifunctional CeO<sub>2</sub>-ATiO<sub>2</sub> nanofiller and incorporated it into bare SPEEK membranes to prepare hybrid SPEEK/CeO<sub>2</sub>-ATiO<sub>2</sub> membranes. The large

surface area of ATiO<sub>2</sub> nanorods facilitated the homogeneous hydrothermal coating of CeO<sub>2</sub>, which endowed the hybrid membranes with the ability to scavenge free radicals. In addition, the functionalized amine groups of ATiO<sub>2</sub> increased proton conductivity of the membrane via a proton hopping mechanism leading to enhanced PEMFC performance under low RH conditions. At the same time, as the surface hydroxyl groups (OH) presented in the ATiO<sub>2</sub> nanorods and CeO<sub>2</sub> have high water retention capability and could offer an additional proton transfer pathway via increased bound water content.

## 2 | EXPERIMENT

### 2.1 | Materials

PEEK pellets were obtained from Victrex Company. Sulfuric acid (H<sub>2</sub>SO<sub>4</sub>, 95%) was procured from Daejung Chemicals, South Korea. Titanium tetraisopropoxid (TTIP) and oxalic acid were purchased from Sigma Aldrich. Sodium hydroxide (NaOH) and cerium nitrate hexahydrate [Ce(NO<sub>3</sub>)<sub>3</sub>·6H<sub>2</sub>O] were obtained from Acros Organics. Toluene anhydrous, 3-aminopropyltriethoxysilane (APTES, 99%), dimethyl sulfoxide (DMSO, 99%), and ethanol were acquired from Samchun Chemicals, South Korea.

### 2.2 | Sulfonation of PEEK

The post-sulfonation process of PEEK was done by following the method described by Liu et al<sup>33</sup> Approximately, 20 g of dried PEEK pellets were gradually added to 200 mL of H<sub>2</sub>SO<sub>4</sub> then the mixture was vigorously agitated using a mechanical stirrer (500 rpm) at 40°C until complete dissolution of PEEK. Afterward, the temperature of the solution was increased to 60°C for 2 hours. The sulfonation process was ended by adding the homogeneous polymer mixture into a flask containing cold water. Finally, the obtained SPEEK fibers were washed continuously with deionized (DI) water until a neutral pH was achieved and were dried in an oven at 80°C for 12 hours.

### 2.3 | Hydrothermal synthesis of TiO<sub>2</sub> nanorods

A hydrothermal fabrication strategy was employed to prepare TiO<sub>2</sub> nanorods. First, 0.182 M of TTIP and 0.364 M of oxalic acid were dissolved in 40 mL of DI water. Then 16 g

of NaOH solution was added to the solution. After an hour of stirring at room temperature (RT), a viscous white solution was obtained, which was poured into a container that was then placed in a tightly sealed autoclave and kept in a vacuum oven at 150°C for 48 hours. Finally, the synthesized white precipitates of TiO<sub>2</sub> nanorods were purified by washing with 0.1 M of HCl then DI water, and subsequently dried in an oven at 80°C for 12 hours.

## 2.4 | Chemical functionalization of APTES on TiO<sub>2</sub> nanorods

A two-stage simple chemical reaction was executed to graft amine groups onto TiO<sub>2</sub> nanorods. Initially, 0.25 g of TiO<sub>2</sub> nanorods was dispersed in 100 mL of anhydrous toluene via ultrasonication at RT for 1 hour. Then, to functionalize the NH<sub>2</sub> moieties on the TiO<sub>2</sub> nanorods, 8 mL of APTES was slowly added to the solution mixture and refluxed under an inert atmosphere at 120°C for 24 hours. Finally, the solution was centrifuged and the obtained ATiO<sub>2</sub> was washed continuously with DI water followed by ethanol and then dried at 80°C for 12 hours.

## 2.5 | Fabrication of ATiO<sub>2</sub>-CeO<sub>2</sub>

Nanofillers of ATiO<sub>2</sub>-CeO<sub>2</sub> were synthesized by adopting a hydrothermal method. Briefly, 0.1 g of ATiO<sub>2</sub> was dispersed in 25 mM of Ce(NO<sub>3</sub>)<sub>3</sub>·6H<sub>2</sub>O solutions, then the mixture was stirred at 60°C for 2 hours. Afterward, 20 mL of 1-M NaOH solution was carefully added into the mixture and the stirring was continued for another 3 hours. Then, the solution mixture was transferred into a 70-mL autoclave and kept in a vacuum oven at 150°C for 18 hours. Finally, the obtained CeO<sub>2</sub>-ATiO<sub>2</sub> nanofiller was washed continuously with DI water and followed by ethanol then dried in an oven at 80°C for 12 hours. It is worthwhile to mention that the white color of synthesized TiO<sub>2</sub> powder is subsequently changed into yellowish after the amine-functionalization process.

## 2.6 | Preparation of composite membrane

Bare SPEEK, SPEEK/TiO<sub>2</sub>, and SPEEK/CeO<sub>2</sub>-ATiO<sub>2</sub> composite membranes were prepared via a solution casting method. Briefly, 0.5 g of SPEEK fibers was dissolved in 10 mL of DMSO. Then, CeO<sub>2</sub>-ATiO<sub>2</sub> at various weight ratios (0.5%, 1%, 2%, 4%, or 6%) was added to the polymer solution. Subsequently, the solution mixture was

sonicated for homogeneous dispersion of CeO<sub>2</sub>-ATiO<sub>2</sub> and followed by agitation at 80°C for 12 hours. The mixture was then cast onto a glass petri dish having a diameter of 0.7 cm and was placed in a vacuum oven at 80°C for 12 hours. Afterward, the membrane was detached from the dish by immersing it in DI water for 1 hour. For comparison, unincorporated SPEEK and SPEEK filled with 2 wt% of bare TiO<sub>2</sub> nanorods were prepared following the same procedure described above. A digital micrometer was used to measure the thickness of the membranes and all prepared membranes were 90 μm ± 0.5 μm thick. The schematic in Figure 1 shows the synthesis route of SPEEK/CeO<sub>2</sub>-ATiO<sub>2</sub> membranes.

## 3 | CHARACTERIZATION

High-resolution transmission electron microscopy (HR-TEM), field emission scanning electron microscopy (FE-SEM), and normal SEM were adopted to study the morphological properties of prepared samples using Supra 40VP (ZEISS), JEM-2010 (JEOL), and JSM-6400 (JEOL) microscopes, respectively. The chemical properties of nanofillers and membranes were investigated by X-ray diffractometer (XRD) (PANalytical X'Pert Pro powder) and Fourier transform infrared (FT-IR) spectroscopy (spectrum GX model spectrometer) in the frequency range of 4000 to 400 cm<sup>-1</sup>. The surface morphology of fabricated membranes was studied by SEM using platinum as a sputtering material. Surface topological properties of fabricated membranes were studied using an atomic force microscope (AFM) (multimode-8 model, Bruker) in contact mode. The contact angle and surface wettability of the membranes were measured by employing a drop shape analyzer (DSA10, Kruss GmbH). Advantage I surface measurement was utilized to conduct the dynamic vapor sorption (DVS) measurement for the membranes. During the DVS, the RH-dependent water absorption and desorption analysis of membranes conducted at a 10% RH interval. Thermal stabilities of synthesized membrane samples were evaluated via thermogravimetric analysis (TGA) using a Q50-TA instrument in the temperature range of 25°C to 800°C under an N<sub>2</sub> atmosphere. Additionally, a Q20-TA instrument was employed to perform the differential scanning calorimetry (DSC) analysis of the membranes. Thermomechanical stabilities of the prepared membranes were examined using a dynamic mechanical analyzer (DMA) (Q800-TA instruments) from -50°C to 170°C under an N<sub>2</sub> atmosphere. Universal testing machine (UTM) (LR5K plus 5 kN, Ametek-Lloyd Instruments) was employed to test the tensile strength, and

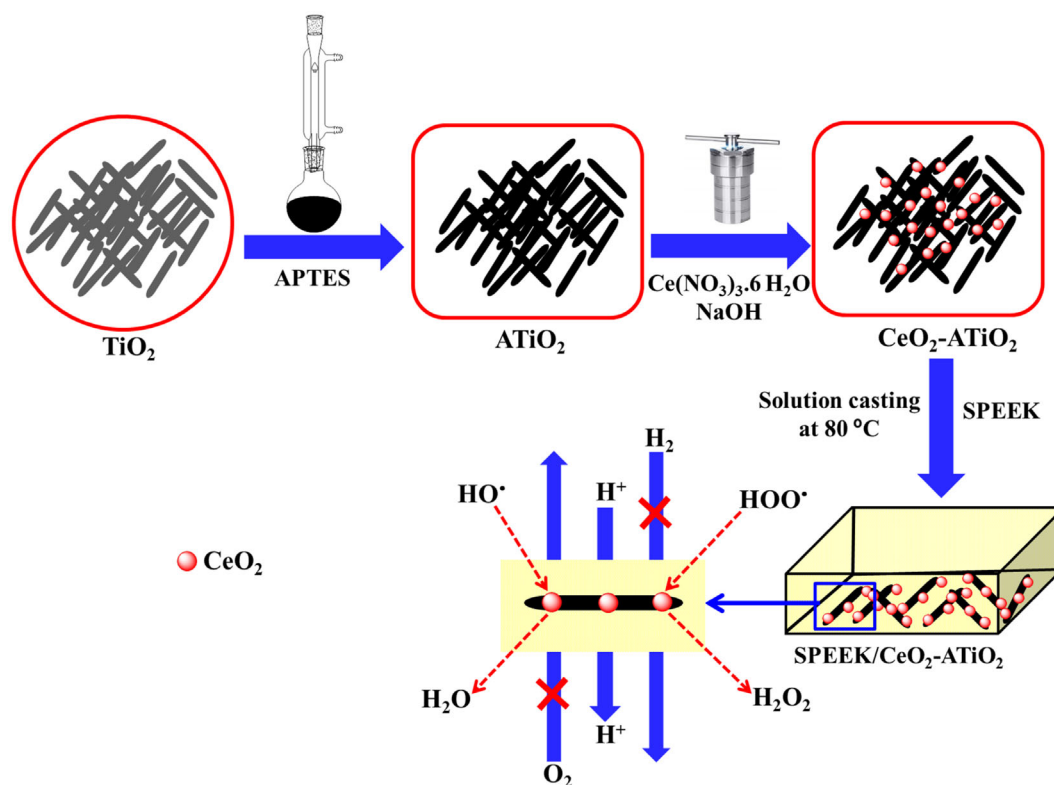


**FIGURE 1** Schematic representation for the preparation of SPEEK/CeO<sub>2</sub>-ATiO<sub>2</sub> composite membrane. APTES, 3-aminopropyltriethoxysilane; SPEEK, sulfonated poly(ether ether ketone)

elongation at break of the prepared membranes. To identify the DS, <sup>1</sup>H NMR (Nuclear magnetic resonance spectroscopy) experiments were conducted using JNM-ECZ600R (JEOL Ltd) equipment. All the aforementioned equipment and measurements were installed and conducted in the Center for University-wide Research Facilities (CURF) at Jeonbuk National University.

## 4 | MEASUREMENTS

### 4.1 | Water uptake and swelling ratio

Water uptake and swelling ratio were assessed by measuring dimensional changes in the weight and thickness of dry and wet membranes.<sup>34,35</sup> Before conducting the measurements, the prepared membranes were dried in an oven at 90°C for 12 hours. Weight ( $W_{\text{dry}}$ , g) and thickness ( $T_{\text{dry}}$ , mm) of the dried membranes were measured and samples were then immersed in a DI water container at 60°C for 24 hours. Afterward, surface water on the wet membranes was removed using blotting paper and then the weight ( $W_{\text{wet}}$ , g) and thickness ( $T_{\text{wet}}$ , mm) of the membranes were measured. Finally, the water uptake and the swelling ratio of membranes were calculated

using Equations (1) and (2). Measurements were taken three times to ensure repeatability of values.

$$\text{Water uptake (\%)} = \left[ \frac{W_{\text{wet}} - W_{\text{dry}}}{W_{\text{dry}}} \right] \times 100\% \quad (1)$$

$$\text{Swelling ratio (\%)} = \left[ \frac{T_{\text{wet}} - T_{\text{dry}}}{T_{\text{dry}}} \right] \times 100\% \quad (2)$$

### 4.2 | Ion exchange capacity

Ion exchange capacity (IEC) measurement was conducted to estimate the number milliequivalents of ions presenting in the dry membranes. Firstly, to exchange all the H<sup>+</sup> ions with Na<sup>+</sup>, the prepared dry membranes were soaked in 0.1-M NaCl for 24 hours. Then, the 0.01 M of NaOH was used to titrate the above solution by utilizing the phenolphthalein as an indicator. Finally, by carefully monitoring the volume of consumed NaOH solution during the titration, the molar quantity of ionic groups in the prepared membranes were determined. To ensure the repeatability of the values, the measurements were repeated several times. The equation for the calculation of IEC values is shown below.

$$\text{IEC} = \frac{\text{Volume of NaOH consumed} \times \text{Concentration of NaOH}}{\text{Weight of the dry membrane}} \quad (3)$$

### 4.3 | Oxidative stability

Fenton's test was performed to determine the oxidative stability of the membranes.<sup>35</sup> Initially, Fenton's reagent was prepared by adding a small fraction of FeSO<sub>4</sub> (2 ppm) into 3% H<sub>2</sub>O<sub>2</sub> solution, and dried samples were submerged in the reagent at 60°C until visible membrane degradation. Degradation time and residual weight of the samples were used to calculate oxidative stability.

### 4.4 | Proton conductivity

A four-probe cell (Bekk-Tech) was utilized to measure resistance ( $R$ ,  $\Omega$ ) of prepared membranes by the alternative current impedance spectroscopy. An appropriate area ( $A$ , cm<sup>2</sup>) of membrane sample (3 cm × 0.5 cm) was fixed into the cell in the longitudinal direction and then the RH-dependent proton conductivity ( $\sigma$ , mS cm<sup>-2</sup>) was calculated using Equation (4).<sup>36,37</sup>

$$\sigma \text{ (mS cm}^{-2}\text{)} = \frac{L}{RTW} \quad (4)$$

In this equation,  $L$ ,  $T$ , and  $W$  are the distance between the four probes, the thickness of the membrane sample, and the width of the membrane sample, respectively.

### 4.5 | Preparation of MEA and evaluation of single-cell performance and durability

MEA was prepared by hot pressing the prepared membranes with commercially available gas diffusion electrodes (GDEs, 0.3 mg cm<sup>-2</sup> Pt loading) on both sides at 70°C under 80 bar for 2.5 minutes. Prior to the voltage-current-resistance (VIR) measurements, the MEA was activated for 6 hours at 0.6 V and a temperature of 60°C. Afterward, the current density and the power density of the membranes were measured by maintaining constant voltage under 100% RH and 30% RH at 60°C. The flow rates of H<sub>2</sub> and O<sub>2</sub> were maintained as 100 and 300 mL min<sup>-1</sup> without applying further backpressure. The RH in the cell was modified by varying pre-heater and saturated temperatures. The durability of MEAs was examined by maintaining an open circuit voltage (OCV) at 60°C under 30% RH. OCV degradation of MEAs was evaluated as a function of time up to 100 hours.

## 5 | RESULTS AND DISCUSSION

### 5.1 | Properties of nanofillers

The APTES is used to graft amine (NH<sub>2</sub>) moieties on the surface of prepared TiO<sub>2</sub> nanorods. Briefly, during the amine-functionalization process, the nucleophilic surface OH groups of TiO<sub>2</sub> attack the ethoxysilane of APTES that resulting in the condensation of OH where the Si-O-Ti bond is formed by releasing ethanol as a byproduct. To ensure the abovementioned formation, the chemical properties of nanofillers were examined by observing FT-IR spectra shown in Figure S1. The peaks presented below 700 cm<sup>-1</sup> were ascribed to the existence of Ti-O and Ti-O-Ti moieties of TiO<sub>2</sub> nanorods.<sup>31,38</sup> A wide peak at 3386 cm<sup>-1</sup> and a small peak at 1662 cm<sup>-1</sup> can be ascribed to the bending and stretching vibrations of OH groups and absorbed water on the surface of TiO<sub>2</sub> nanorods and CeO<sub>2</sub>. The length of the wide peak at 3386 was reduced in the case of CeO<sub>2</sub>-ATiO<sub>2</sub> due to the condensation of OH groups of TiO<sub>2</sub> during the NH<sub>2</sub> functionalization. Successful functionalization of NH<sub>2</sub> groups on TiO<sub>2</sub> can be further demonstrated by the presence of peaks at 2928, 2864, and 1510 cm<sup>-1</sup> attributed to symmetric and asymmetric vibration stretching of the C-H and -CH<sub>2</sub> bonds of APTES.<sup>38</sup> The peaks at 1030 and 1125 cm<sup>-1</sup> were ascribed to Si-O-Si bond stretching of APTES. The observed peak at 910 cm<sup>-1</sup> is confirming the formation of the Si-O-Ti bond.<sup>38</sup> Compared to the pure TiO<sub>2</sub>, a new peak at 700 cm<sup>-1</sup> was presented in CeO<sub>2</sub>-ATiO<sub>2</sub> nanofillers due to the CeO<sub>2</sub> stretching.<sup>32</sup> Furthermore, the XRD patterns of TiO<sub>2</sub> and CeO<sub>2</sub>-ATiO<sub>2</sub> were displayed in Figure S2. The XRD patterns of TiO<sub>2</sub> are consistent with the previously reported literature.<sup>39</sup> Hence, it is assumed that the prepared TiO<sub>2</sub> nanorods consist of both rutile and anatase phases, whereas the CeO<sub>2</sub> has cubic fluorite structure. The two new peaks at 60° and 80° can be ascribed to the CeO<sub>2</sub> nanoparticles for CeO<sub>2</sub>-ATiO<sub>2</sub>. Figure S3 shows FE-SEM and TEM images of TiO<sub>2</sub>, ATiO<sub>2</sub>, and CeO<sub>2</sub>-ATiO<sub>2</sub> and their corresponding Energy-dispersive X-ray spectroscopy (EDAX) spectra. As shown in Figure S3a and d, TiO<sub>2</sub> nanorods were uniformly distributed owing to the repulsive interactions between surface OH moieties of TiO<sub>2</sub>. This uniformity of TiO<sub>2</sub> nanorods was unchanged even after NH<sub>2</sub> functionalization (ATiO<sub>2</sub>), indicating that the NH<sub>2</sub> moieties did not alter the morphology of TiO<sub>2</sub> (Figure S3b and e). Grafted CeO<sub>2</sub> nanoparticles were randomly scattered on the surface of TiO<sub>2</sub>, leading to exposure of NH<sub>2</sub>, OH, and CeO<sub>2</sub> groups (Figure S3c and f). When incorporated into the membrane, the exposure of the surface OH and NH<sub>2</sub> groups of CeO<sub>2</sub> and ATiO<sub>2</sub> can improve proton conductivity via bound water and water-free proton transfer,

respectively. Besides, the scattered  $\text{CeO}_2$  particles can scavenge radicals under the harsh PEMFC environment without blocking the function of  $\text{NH}_2$  and  $\text{OH}$  groups. Additionally, EDAX spectra, Figure S3g-i, showed that carbon, oxygen, silicon, cerium, titanium, and nitrogen were all present in the  $\text{CeO}_2$ - $\text{ATiO}_2$  nanofiller. Those above-mentioned morphological phenomena can also be seen in HR-TEM images and the corresponding EDAX spectra of  $\text{CeO}_2$ - $\text{ATiO}_2$  shown in Figure S4. Cumulatively, the abovementioned chemical and physical properties of the prepared nanofiller are demonstrating the successful formation of the desired  $\text{CeO}_2$ - $\text{ATiO}_2$ .

## 5.2 | Structural and chemical properties of membranes

$^1\text{H}$  NMR was employed to analyze the DS of prepared SPEEK membranes. The  $^1\text{H}$  NMR graph displayed in Figure S5 illustrates the aromatic hydrogen peaks of SPEEK from  $\text{H}_1$  to  $\text{H}_{14}$ . The DS of SPEEK was determined to be 66.6% based on the equation below.<sup>33</sup>

$$\text{DS} = \frac{12}{(A_{\text{H}1,2,3,4} + A_{\text{H}6,7,8,9,10,11,12,13,14}/A_{\text{H}5} + 2)} \times 100\% \quad (5)$$

The structural chemical properties of SPEEK and SPEEK/ $\text{CeO}_2$ - $\text{ATiO}_2$  (2%) was examined by XRD and FT-IR patterns as presented in Figures S6 and S7. It is found

that the incorporation of the  $\text{CeO}_2$ - $\text{ATiO}_2$  into the SPEEK membrane did not alter the chemical structure of the polymer matrix since the XRD and FT-IR patterns merely showed any differences. As shown in Figure S6, both membranes displayed a broad peak at  $2\theta$  of  $20^\circ$  to  $21^\circ$  that can be attributed to the diminished crystallinity of the PEEK from semicrystalline to amorphous after the sulfonation process.<sup>40-42</sup> This result is well versed with the NMR result of bare SPEEK conforming the successful functionalization of sulfonic acid ( $\text{SO}_3\text{H}$ ) moieties.<sup>31,43,44</sup> In the XRD spectra, it can be seen that the width of the broad peak is unchanged for the SPEEK/ $\text{CeO}_2$ - $\text{ATiO}_2$  membrane demonstrating the incorporation of  $\text{CeO}_2$ - $\text{ATiO}_2$  did not further alter the amorphous property of the SPEEK matrix. However, in the case of FT-IR (Figure S7), the peak of  $\text{OH}$  groups and absorbed water at  $3250\text{ cm}^{-1}$  is slightly widened for the SPEEK/ $\text{CeO}_2$ - $\text{ATiO}_2$  composite membrane owing to the presence of surface  $\text{OH}$  groups of  $\text{CeO}_2$ - $\text{ATiO}_2$  nanofiller. That further depicting the successful incorporation of the nanofiller into bare membrane.

## 5.3 | Morphological properties of membranes

The surface FE-SEM images of SPEEK and SPEEK/ $\text{CeO}_2$ - $\text{ATiO}_2$  (2%) with corresponding Energy-dispersive X-ray spectroscopy (EDX) spectra are provided in Figure 2.

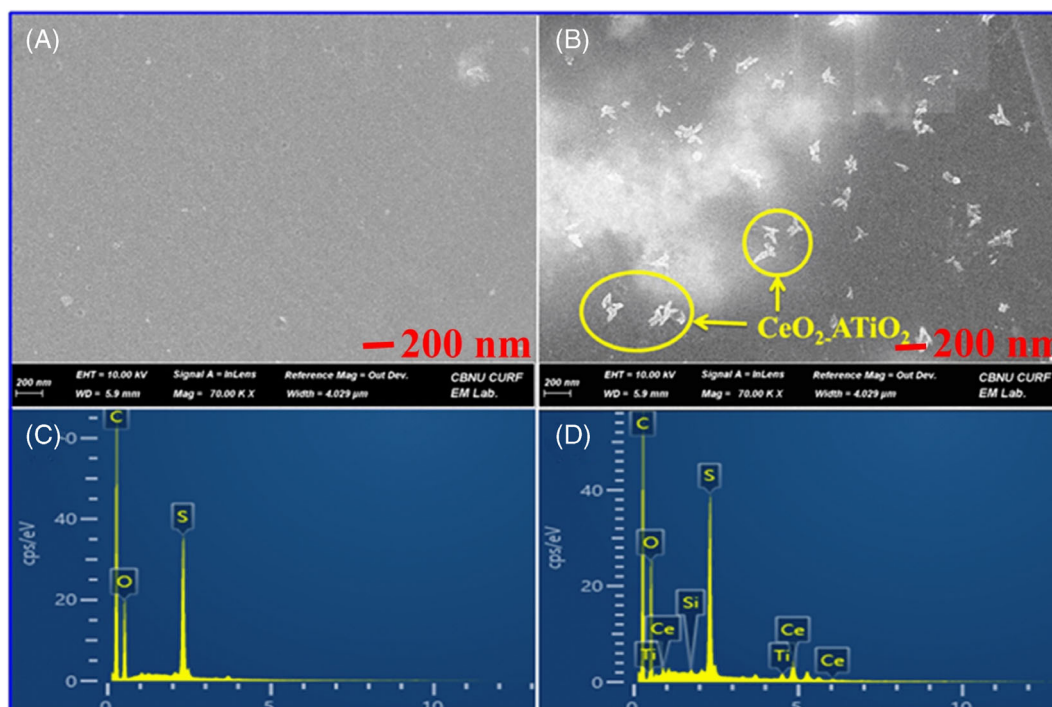


FIGURE 2 FE-SEM images and corresponding EDX spectra of (A) and (C) bare SPEEK and (B) and (D) SPEEK/ $\text{CeO}_2$ - $\text{ATiO}_2$  nanocomposite membrane. FE-SEM, field emission scanning electron microscopic; EDX, Energy-dispersive X-ray spectroscopy

Surface FE-SEM images reveal that the bare SPEEK membrane had a smooth surface without any cracks or surface damages. In contrast, the surface of the SPEEK/CeO<sub>2</sub>-ATiO<sub>2</sub> (2%) membrane was rough with the presence of nanoparticles, indicating the incorporation of CeO<sub>2</sub>-ATiO<sub>2</sub> nanofillers into the SPEEK matrix. Additionally, the EDAX spectra of SPEEK/CeO<sub>2</sub>-ATiO<sub>2</sub> membranes show the peaks of cerium (Ce), titanium (Ti), silicon (Si), carbon (C), oxygen (O), and sulfur (S) while the bare SPEEK membrane only had peaks of C, O, and S (Figure 2C,D). Besides, it confirms that the 2% weight incorporation of CeO<sub>2</sub>-ATiO<sub>2</sub> did not decrease the density of sulfuric acid present in SPEEK. Additionally, the cross-sectional FE-SEM images of prepared membranes were obtained to verify the incorporation and existence of CeO<sub>2</sub>-ATiO<sub>2</sub> nanofiller in the SPEEK membrane. Figure 3 displays the cross-sectional FE-SEM images of SPEEK and SPEEK/CeO<sub>2</sub>-ATiO<sub>2</sub> (2 wt%) membranes. Before conducting the cross-sectional FE-SEM analysis, the membrane samples were freeze-dry cut by dipping into the nitrogen liquid. As shown in Figures 3B, D, and F, the CeO<sub>2</sub>-ATiO<sub>2</sub> nanoparticles were present in the

composite membrane making its cross-sectional surface rough while the bare SPEEK membrane showed clear and unfilled cross section (Figure 3A, C, and E). The existence of CeO<sub>2</sub>-ATiO<sub>2</sub> nanofiller can also be seen in the selected area SEM image of SPEEK/CeO<sub>2</sub>-ATiO<sub>2</sub> (2%) membrane (Figure 4A). Also, from the EDAX spectra and elemental mapping, the presence of elements such as C, O, Si, S, Ti, and Ce is confirmed in the composite membrane as displayed in Figure 4. Two-dimensional and three-dimensional AFM surface images of SPEEK and SPEEK/CeO<sub>2</sub>-ATiO<sub>2</sub> membranes are shown in Figure 5. Pristine SPEEK had a smooth surface with almost no roughness due to the physical nature of the SPEEK polymer (Figure 5A, C, and E). In contrast, SPEEK/CeO<sub>2</sub>-ATiO<sub>2</sub> nanocomposite membranes had a higher surface roughness because of distribution of nanofiller throughout the membrane. The performance of PEMFCs is highly dependent on interactions among the GDL, catalyst, and membrane are known as three phase boundary regions.<sup>18,25</sup> Hence, the enhanced interface of three phase regions improves the performance outputs of PEMFCs. In that regard, a composite

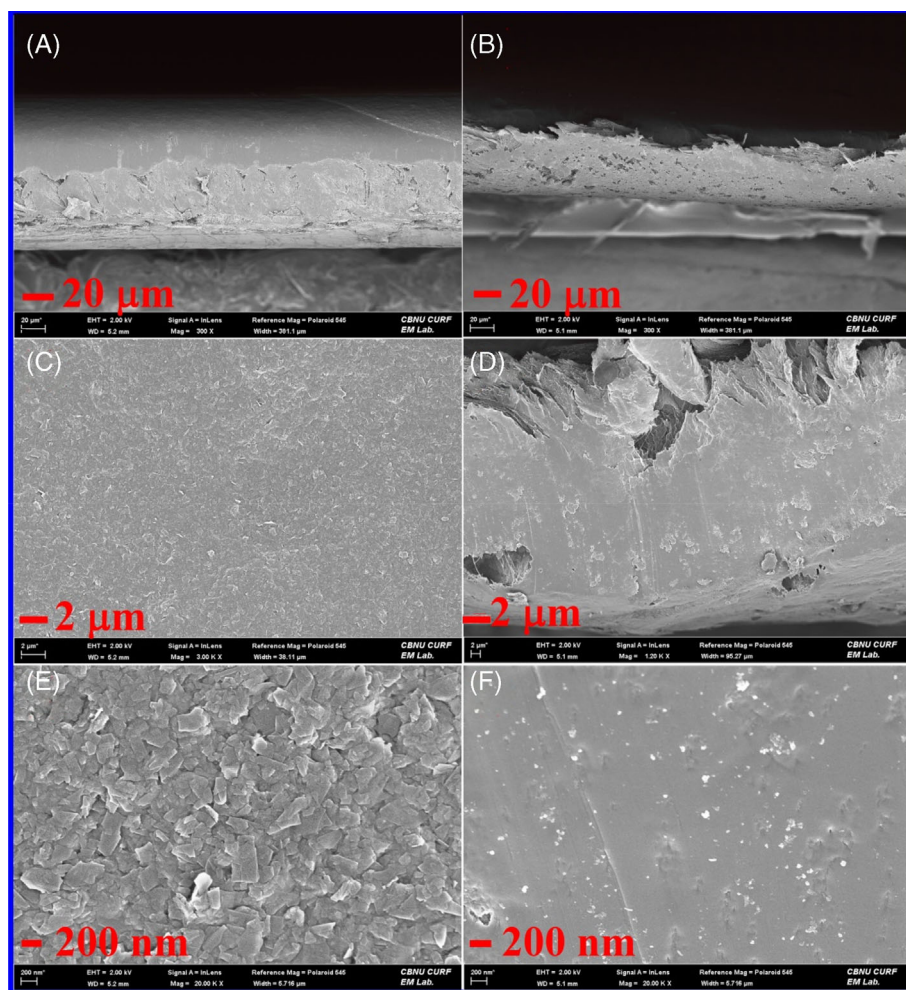
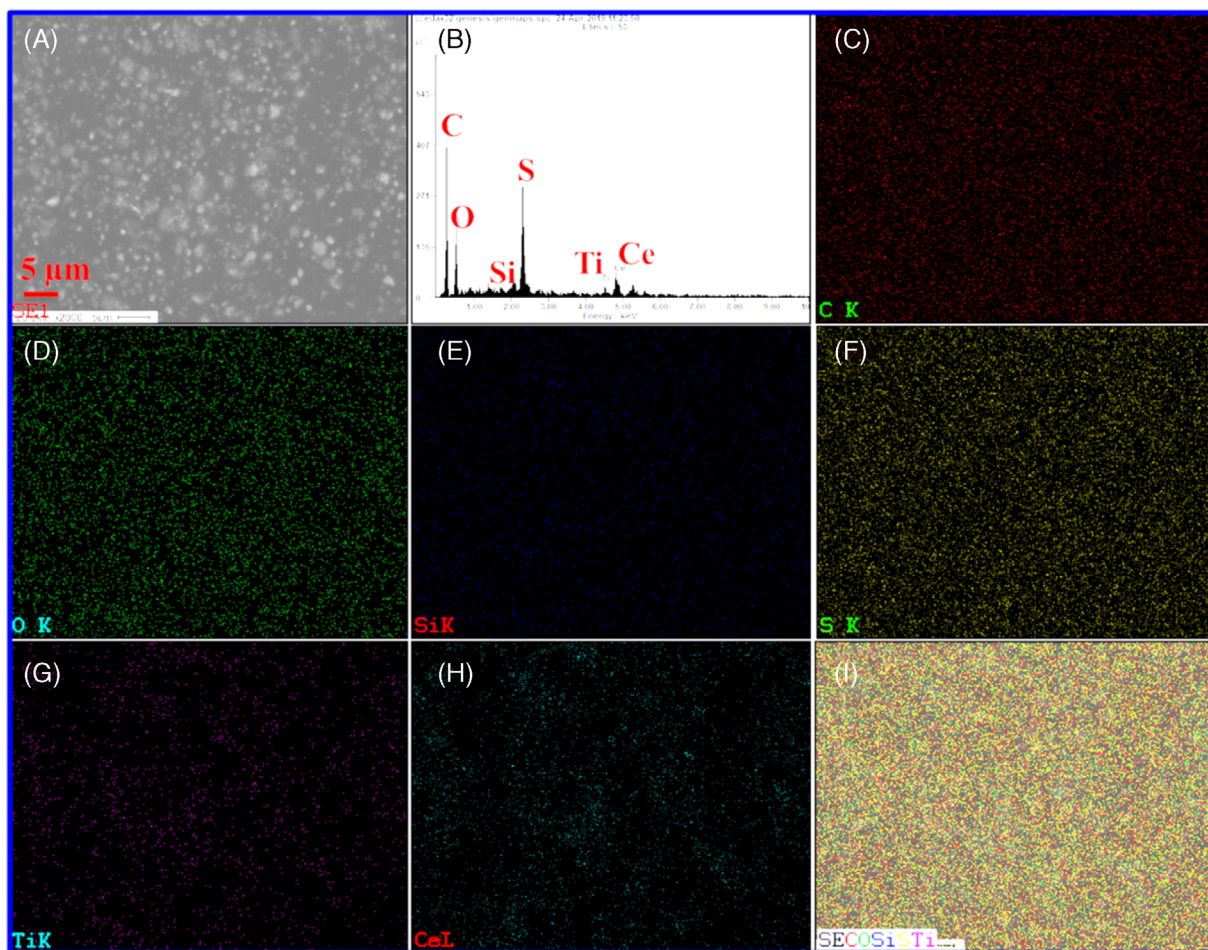


FIGURE 3 Cross-sectional FE-SEM images of (A), (C), and (E) bare SPEEK and (B), (D), and (F) SPEEK/CeO<sub>2</sub>-ATiO<sub>2</sub> nanocomposite membrane. FE-SEM, field emission scanning electron microscopic





**FIGURE 4** (A) Selected area SEM image and (B) corresponding EDAX spectra of nanocomposite membrane; elemental mapping of (C) carbon, (D) oxygen, (E) silicon, (F) sulfur, (G) titanium, (H) cerium, and (I) overlapping of all elements. SEM, scanning electron microscopic

membrane with a rougher surface is more compatible with the GDE creating an effective three phase interaction.<sup>37</sup> Surface morphological studies of the prepared membranes clearly demonstrate the successful incorporation of  $\text{CeO}_2\text{-ATiO}_2$  nanofiller into the SPEEK matrix.

#### 5.4 | Physiochemical and electrochemical properties of membranes

Physiochemical properties of the membranes such as water uptake with swelling ratio, the contact angle with surface wettability, and water sorption were studied and the corresponding results are presented in Figures 6 and S8a. Water uptake of the SPEEK/ $\text{CeO}_2\text{-ATiO}_2$  nanocomposite membranes showed a decreasing pattern as the weight ratio of nanofiller is increased, which due to the nonwater conducting nature of  $\text{ATiO}_2$ . Membrane swelling is an important characteristic of PEMs since the high swelling leads to membrane failure eventually to the

PEMFC system failure.<sup>26</sup> Compared to the bare SPEEK membrane, all composite membranes displayed a low degree of swelling. This behavior of the SPEEK/ $\text{CeO}_2\text{-ATiO}_2$  membranes can be attributed to the chemical interactions between the SPEEK matrix and the incorporated  $\text{CeO}_2\text{-ATiO}_2$ . The chemical interaction can restrict the dimensional expansion of composite membranes when hydrated, thereby leading to prevent membrane failure.<sup>32</sup> The nonwater conducting phenomena of  $\text{ATiO}_2$  can also be seen in the water absorption and desorption curves of SPEEK and SPEEK/ $\text{CeO}_2\text{-ATiO}_2$  (2%) membranes in Figure 6B. The SPEEK/ $\text{CeO}_2\text{-ATiO}_2$  membrane exhibited slightly lower water absorption and desorption patterns than the bare SPEEK membrane since the  $\text{ATiO}_2$  did not absorb humidity. The contact angle test was conducted to study the surface wettability of the SPEEK and SPEEK/ $\text{CeO}_2\text{-ATiO}_2$  (2%) membranes and the corresponding results are shown in Figure 6C. Compared to the bare SPEEK ( $33.7 \text{ mN m}^{-1}$  and  $75.66^\circ$ ), the SPEEK/ $\text{CeO}_2\text{-ATiO}_2$  exhibited low wettability and high contact angle ( $20.4 \text{ mN m}^{-1}$  and  $93.75^\circ$ ). The reduction

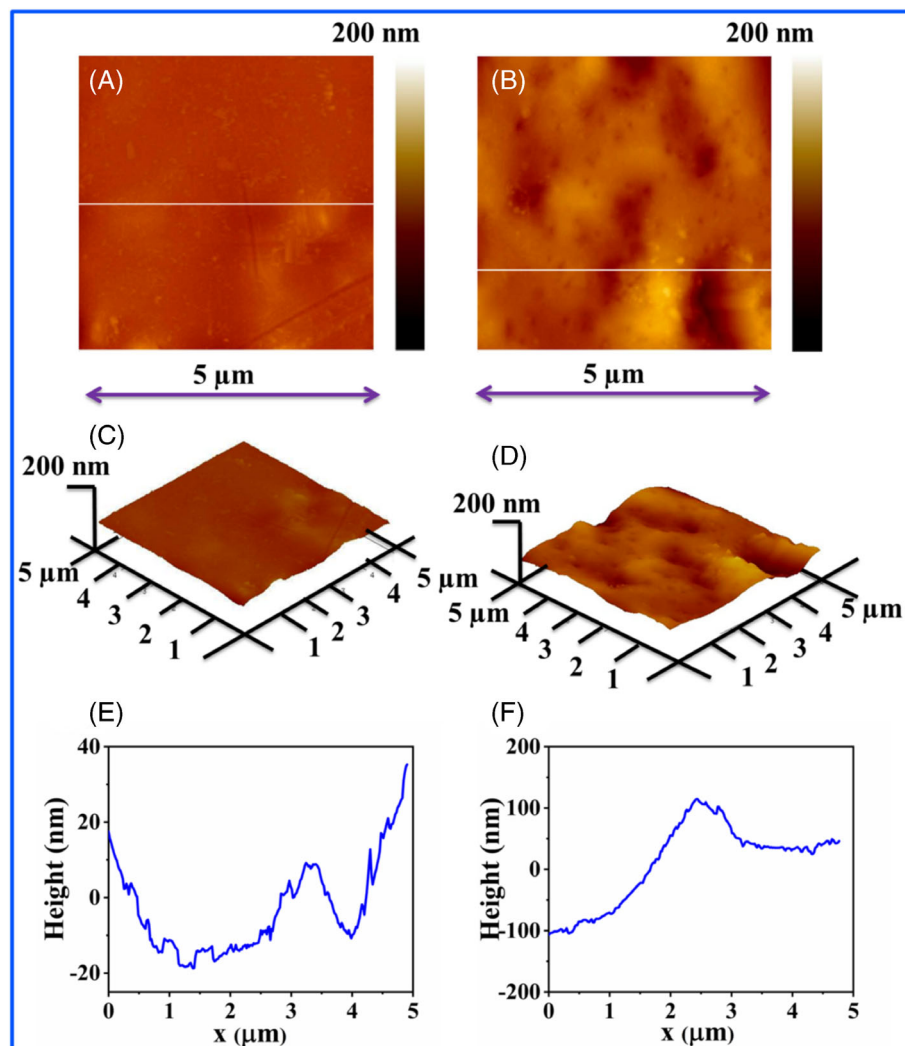


FIGURE 5 AFM two-dimensional surface images, three-dimensional surface images, and line profile of (A), (C), and (E) SPEEK and (B), (D), and (F) SPEEK/CeO<sub>2</sub>-ATiO<sub>2</sub> membranes. AFM, atomic force microscopic; SPEEK, sulfonated poly(ether ether ketone)

in the wettability was properly due to the presence of NH<sub>2</sub> moieties in the composite membrane. However, as mentioned previously, the NH<sub>2</sub> moieties of ATiO<sub>2</sub> can rapidly conduct protons by water-free proton transfer. The IEC values of prepared membranes are given in Table S1. The IEC values of the composite membranes; SPEEK/TiO<sub>2</sub> (2%) and SPEEK/CeO<sub>2</sub>-ATiO<sub>2</sub> (2%) are slightly lower than that of pristine SPEEK. This is due to the incorporation of nanofiller that may dilutes the concentration of SO<sub>3</sub>H sites of the membrane matrix. However, as shown in the SEM-EDAX spectra, 2 wt% addition of CeO<sub>2</sub>-ATiO<sub>2</sub> nanoparticles only merely diluted SO<sub>3</sub>H groups in the SPEEK which is negligible.

Proton conductivity is regarded as a crucial electrochemical property of membranes since it directly impacts the efficiency of PEMFCs.<sup>7,12</sup> In general, proton exchange in sulfonated membranes follows two well-known mechanisms, both can occur simultaneously: (i) vehicular and (ii) Grotthuss mechanisms (as shown in Figure 10). SO<sub>3</sub>H in the membrane can attach with water molecules under

hydrated conditions.<sup>27,29</sup> Such bound water molecules help to transfer protons through a vehicular mechanism by generating hydronium ions (H<sub>3</sub>O<sup>+</sup>) as a vehicle or carrier. However, in the case of Grotthuss conduction, proton hopping is facilitated through the hydrogen bonding formed between the ionic groups. During the PEMFC operation, both the mechanisms co-occur up to 80°C with fully humidified conditions. When increasing temperature or decreasing RH, the Grotthuss conduction starts to dominate owing to the removal of water molecules.<sup>39</sup> The humidity-dependent proton conductivity of membranes at 60°C is shown in Figures 6D and S8b. The proton conductivity of SPEEK/CeO<sub>2</sub>-ATiO<sub>2</sub> composite membranes can follow three-way rapid proton transfer induced from the amine derivatives, SO<sub>3</sub>H groups, and the increased bound water content offered by OH groups of incorporated CeO<sub>2</sub>-ATiO<sub>2</sub> nanofiller. The NH<sub>2</sub> moieties of ATiO<sub>2</sub> and SO<sub>3</sub>H groups of SPEEK forms acid–base interactions and transfer the protons via protonation–deprotonation sequence without the aid of water.<sup>45</sup> As a result, the

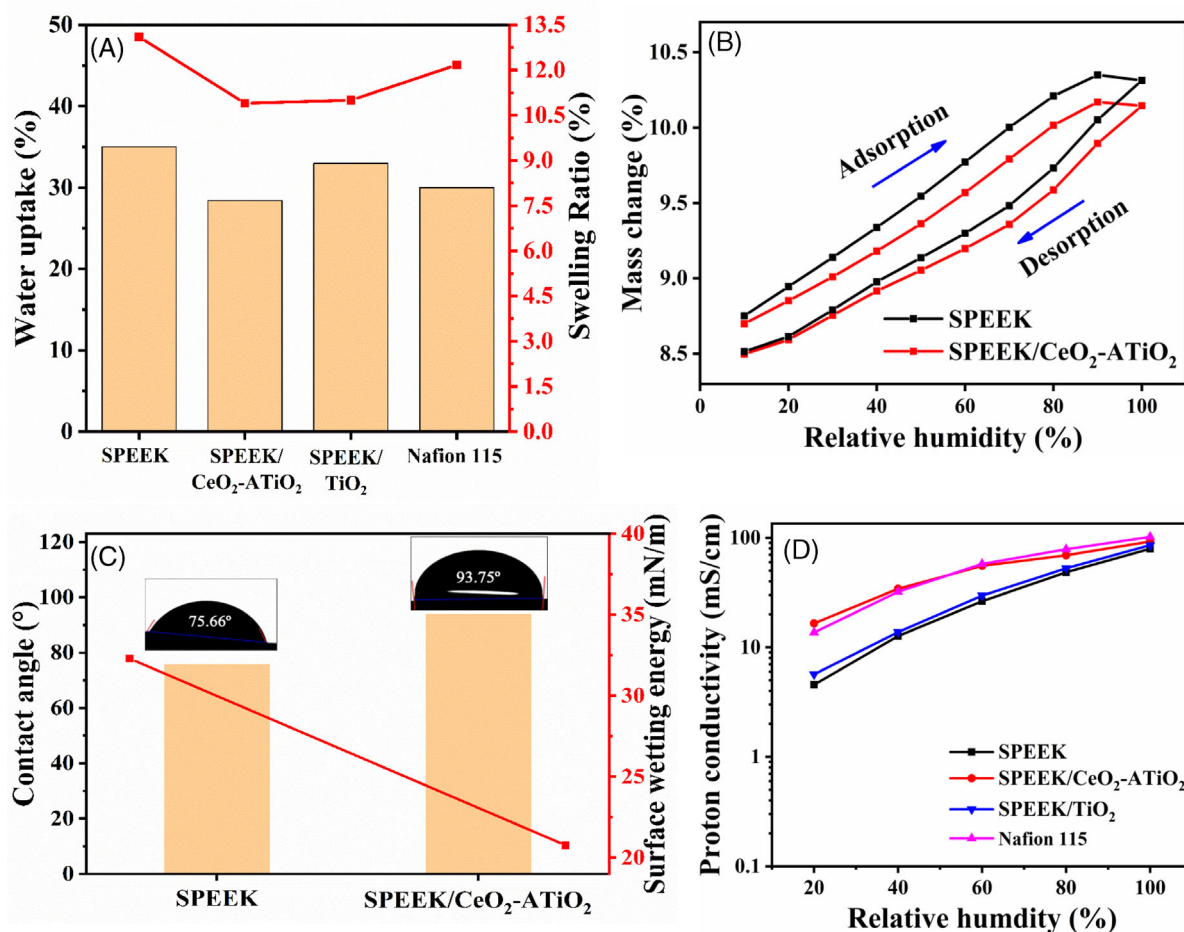


FIGURE 6 A) Water uptake and swelling ratio, (B) water absorption-desorption curves, (C) contact angle with surface wetting energy, and (D) proton conductivity of membranes at 60°C as a function of humidity

composite membranes with various wt% (0.5, 1, 2, 4, and 6) of CeO<sub>2</sub>-ATiO<sub>2</sub> displayed high proton conductivity values than bare SPEEK membrane under low RH conditions up to 80%. However, under 100% RH, the SPEEK/CeO<sub>2</sub>-ATiO<sub>2</sub> membrane with 4 and 6 wt% showed lower proton conductivity values that because of incorporating the high weight ratio of nanoparticles was diluted the density of SO<sub>3</sub>H groups of the SPEEK membrane (Figure S8b). Among all prepared membranes, the SPEEK/CeO<sub>2</sub>-ATiO<sub>2</sub> with 2-wt% nanofiller showed the highest proton conductivity of 92.567 mS cm<sup>-1</sup> at 60°C under 100% RH equaling state-of-the-art Nafion 115, whereas the proton conductivity of pristine SPEEK was 79.37 mS cm<sup>-1</sup> under identical conditions (Figure 6D). This superior performance of the composite membrane was offered by the uniform distribution of CeO<sub>2</sub>-ATiO<sub>2</sub> nanoparticles along the SPEEK matrix. Therefore, when installed into the PEMFC device, the effective proton-conducting ability of the SPEEK/CeO<sub>2</sub>-ATiO<sub>2</sub> (2 wt%) membrane would be beneficial for improving the overall current and power outputs.

## 5.5 | Thermal properties of prepared membranes

The thermal stability of membranes used in PEMFCs directly influences the durability of the MEA.<sup>9,13</sup> An efficient membrane should possess high thermal tolerance to ensure prolonged operation of MEA, specifically, under low RH conditions. The TGA was performed to study the thermal properties of unfilled SPEEK and SPEEK/CeO<sub>2</sub>-ATiO<sub>2</sub> (2%) membranes, and the TGA results are provided in Figure 7A. SPEEK and SPEEK/CeO<sub>2</sub>-ATiO<sub>2</sub> (2%) membranes showed three distinct thermal degradation stages: (i) weight loss at 80°C to 180°C due to decomposition of absorbed water molecules on the surface of the membranes, (ii) weight loss at 220°C to 470°C due to detachment of SO<sub>3</sub>H groups in the membranes,<sup>26</sup> and (iii) weight loss at above 480°C driven by thermal decomposition of the hydrocarbon backbone.<sup>19</sup> The SPEEK/CeO<sub>2</sub>-ATiO<sub>2</sub> nanocomposite membranes had better thermal stability than pristine SPEEK due to the incorporation of CeO<sub>2</sub>-ATiO<sub>2</sub> nanoparticles. Furthermore, the glass

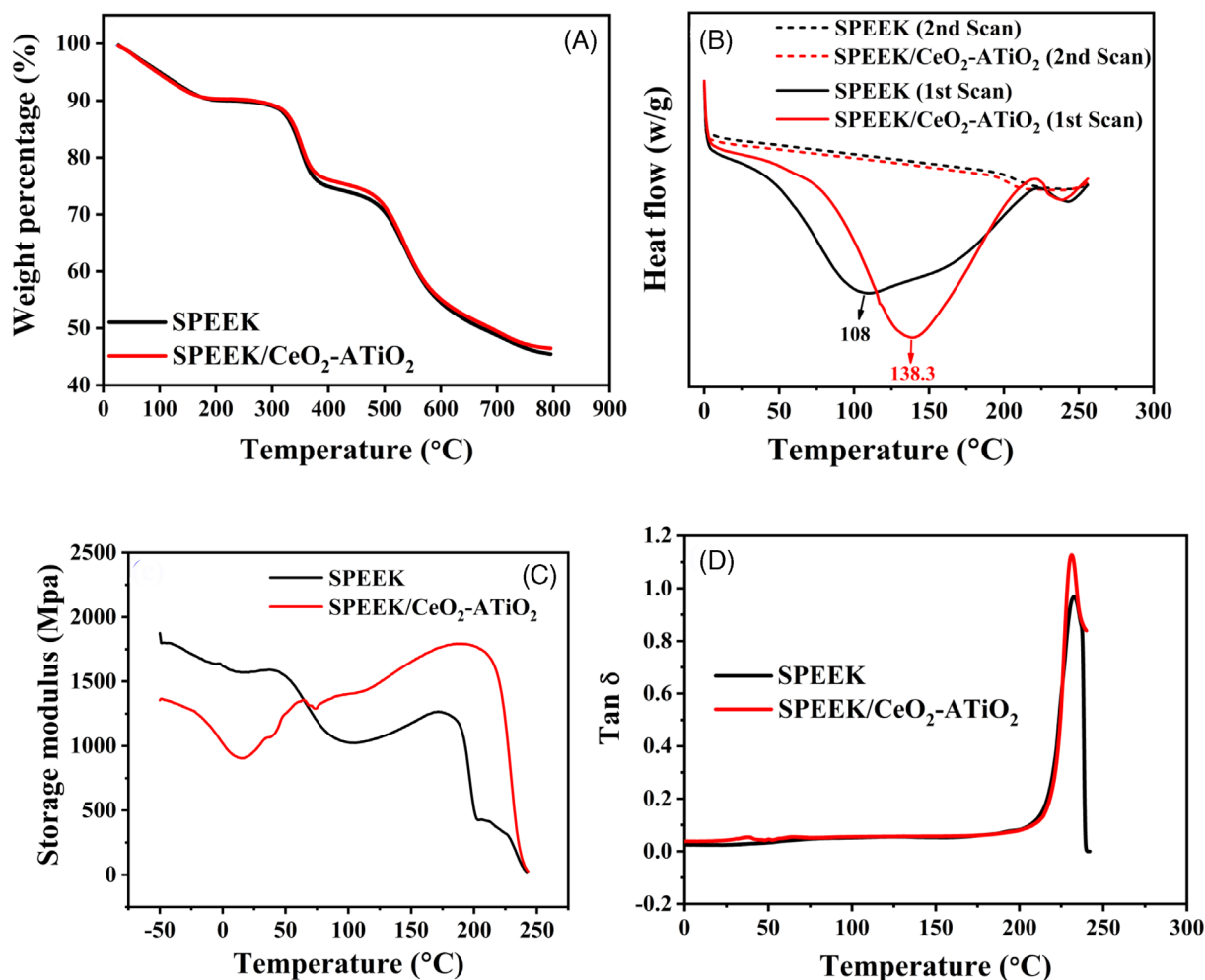


FIGURE 7 Thermomechanical properties SPEEK and SPEEK/CeO<sub>2</sub>-ATiO<sub>2</sub> of membranes: (A) TGA, (B) DSC, (C) and (D) DMA. DMA, dynamic mechanical analyzer; DSC, differential scanning calorimetry; SPEEK, sulfonated poly(ether ether ketone); TGA, thermogravimetric analysis

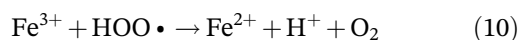
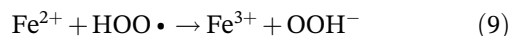
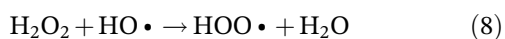
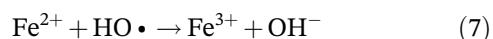
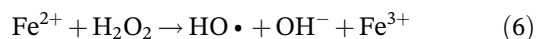
transaction ( $T_g$ ) temperature of SPEEK and SPEEK/CeO<sub>2</sub>-ATiO<sub>2</sub> (2%) membranes was studied via DSC analysis. As shown in Figure 7B, the SPEEK/CeO<sub>2</sub>-ATiO<sub>2</sub> membrane possessed a higher  $T_g$  value of 138.3°C than that of 108°C of the bare membrane. This thermal phenomenon of the SPEEK/CeO<sub>2</sub>-ATiO<sub>2</sub> membrane can be attributed to the strong electrostatic interactions between the nanofiller and membrane matrix that prevented the reformation of polymer chains during heating.

## 5.6 | Thermomechanical and oxidative stability of the membranes

The temperature-dependent mechanical stability of the membranes was assessed using a DMA. Dynamic mechanical analyses evaluate the elastic behavior of membranes by applying a thermomechanical load and then measuring the modulus of storage of the

corresponding membranes.<sup>9</sup> DMA graphs of prepared membranes are presented in Figure 7C,D. SPEEK/CeO<sub>2</sub>-ATiO<sub>2</sub> membrane exhibited a higher modulus of storage than the pristine SPEEK membrane due to chemical interactions such as electrostatic and hydrogen bonding between the nanofiller and polymer matrix in the former. The mechanical properties of the prepared membranes were evaluated by employing a UTM. Figure S9 shows the stress and strain curves of SPEEK and SPEEK/SPEEK/CeO<sub>2</sub>-ATiO<sub>2</sub> (2%) membranes; it is clear that the composite membrane had a higher mechanical strength than the bare membrane. Also, the tensile strength of SPEEK/CeO<sub>2</sub>-ATiO<sub>2</sub> (2 wt%) membrane is slightly higher than that of SPEEK as displayed in Table S2. We attributed this enhancement in mechanical strength to the chain retention property of the composite membrane during stress loading conferred by SPEEK/CeO<sub>2</sub>-ATiO<sub>2</sub>. In brief, strong electrostatic interactions between CeO<sub>2</sub>-ATiO<sub>2</sub> and SPEEK prevented elongation of the polymer

matrix during the test. The higher mechanical strength of SPEEK/CeO<sub>2</sub>-ATiO<sub>2</sub> membranes can enable them to withstand the high mechanical compression of PEMFC stacks during the real-time operation. Fenton's test was utilized to examine the oxidative stability of the membranes. To imitate the PEMFC working environment, the test was conducted at 60°C for 24 hours. Measured residual weights of SPEEK and SPEEK/CeO<sub>2</sub>-ATiO<sub>2</sub> (2%) membranes were 67% and 93%, respectively. During the oxidative test, the addition of Fe derivatives catalyzes the formation of hydroxyl (HO•) and hydroperoxyl (HOO•) radicals in H<sub>2</sub>O<sub>2</sub> solution via the mechanisms shown in Equations (6) to (10) below.<sup>28</sup> SPEEK/CeO<sub>2</sub>-ATiO<sub>2</sub> membranes were not affected by free radicals owing to radical scavenging nature of CeO<sub>2</sub> nanoparticles. Whereas, bare SPEEK membrane lost its weight by 33%, ensuring the vulnerability of sulfonated hydrocarbons to free radicals. However, under real-time PEMFC operation, the generation of radicals is less extreme than in the oxidative test we conducted.



## 5.7 | PEMFC performance and durability

Examination of the OCV and power density of membranes in PEMFCs is crucial to assess the performance outputs of the system.<sup>46</sup> In this study, we examined the

OCV and performance output of a single-cell PEMFC equipped with the MEAs of SPEEK and SPEEK/CeO<sub>2</sub>-ATiO<sub>2</sub> at 60°C under 30% RH and 100% RH. The low RH condition was chosen to assess the stability of membranes under vigorous anhydrous PEMFC operating conditions. In the performance test shown in Figure 8, the SPEEK/CeO<sub>2</sub>-ATiO<sub>2</sub> membrane exhibited a maximum power density of 117 mW cm<sup>-2</sup> at a load current density of 371 mA cm<sup>-2</sup>, which was higher than the power density of 91 mW cm<sup>-2</sup> at a load current of 253 mA cm<sup>-2</sup> attained by bare SPEEK membrane. These results confirmed that the self-humidifying NH<sub>2</sub> functional groups of CeO<sub>2</sub>-ATiO<sub>2</sub> afforded rapid proton conductivity without diluting the SO<sub>3</sub>H ionic domains of SPEEK. The coexistence of SO<sub>3</sub>H and NH<sub>2</sub> improved proton transfer via vehicular and hopping mechanisms, respectively. As mentioned previously, a rough membrane surface improves interactions between the three phase boundaries of MEAs, resulting in improved electrochemical kinetics. Furthermore, the scattered formation of CeO<sub>2</sub> on ATiO<sub>2</sub> resulted in the exposure of all functional groups present in the nanorods, such as OH and NH<sub>2</sub> moieties. The surface OH moieties of TiO<sub>2</sub> and CeO<sub>2</sub> have water absorbing properties, which could improve water retention of the membrane and thus further increase proton transfer by the vehicular mechanism. While the NH<sub>2</sub> moieties of ATiO<sub>2</sub> offer water-free proton conduction via hopping mechanism. As a result, the SPEEK/CeO<sub>2</sub>-ATiO<sub>2</sub> attained a higher PEMFC outputs both under low and fully humidified conditions than the bare SPEEK.

A harsh PEMFC environment can produce acidic radicals such as HO• and HOO•.<sup>36,37</sup> As mentioned earlier, H<sub>2</sub> and O<sub>2</sub> gas-cross over and incomplete O<sub>2</sub> reduction during ORR are responsible for the formation of H<sub>2</sub>O<sub>2</sub>.<sup>47,48</sup> Afterward, the H<sub>2</sub>O<sub>2</sub> molecules react with the metal catalyst (M<sub>cat</sub>) to produce HO• and HOO• radicals which simultaneously attack the vulnerable parts of bare SPEEK matrix and unzip them.<sup>49,50</sup> The formation

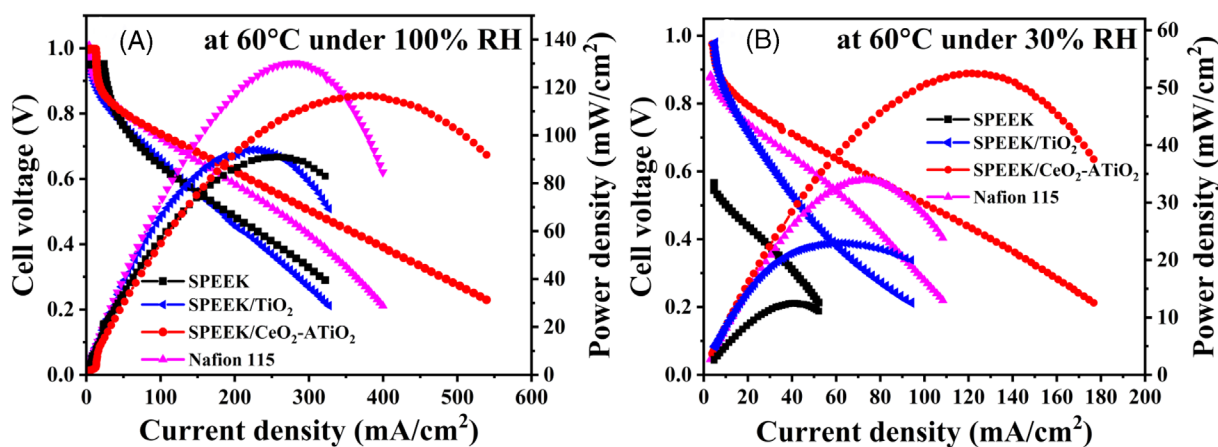
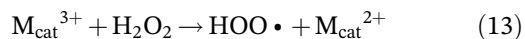
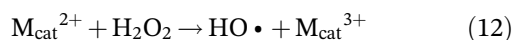
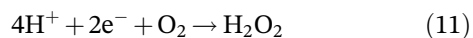


FIGURE 8 Single cell performance graph of membranes conducted under (A) 100% RH and (B) 30% RH. RH, relative humidity

mechanism of those free radicals is depicted in Equations (11) to (13).<sup>36</sup>



Post-sulfonation of PEEK membranes lowers their crystallinity, which in turn decreases the chemical and thermal stability of SPEEK membranes. In addition, the aryl sulfonated and aryl ether bonds of SPEEK membranes are highly vulnerable to the attack by HO• radicals that can scission the membrane matrix, leading to high gas crossover and membrane failure.<sup>22,30</sup> Hence, it is essential to analyze the single-cell durability of the membrane under low RH conditions.

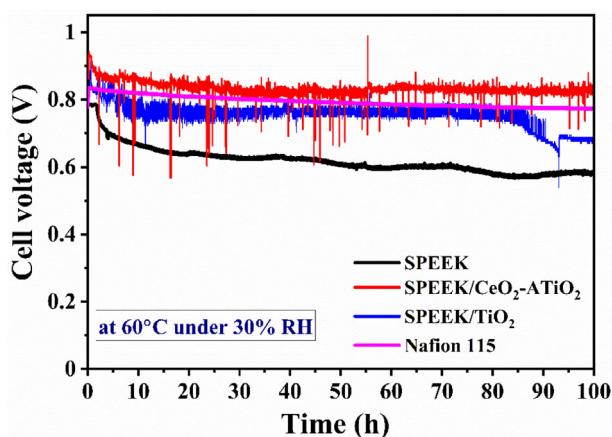
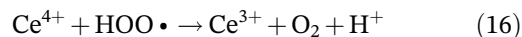
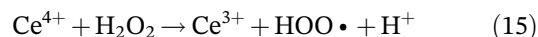
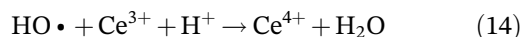


FIGURE 9 OCV curves of membranes conducted at 60°C under 30% RH. OCV, open circuit voltage; RH, relative humidity



The durability curves of membranes, quantified at 60°C under 30% RH over 100 hours, are presented in Figure 9. It exhibited an OCV degradation of  $0.9255 \text{ mV h}^{-1}$  for SPEEK/CeO<sub>2</sub>-ATiO<sub>2</sub> (2 wt%) membrane and  $3.437 \text{ mV h}^{-1}$  for bare SPEEK membrane, a 2.7-fold difference. The CeO<sub>2</sub> in SPEEK/CeO<sub>2</sub>-ATiO<sub>2</sub> promoted the conversion of HO• and HOO• radicals into harmless products, as illustrated in Equations (14) to (16) and Figure 10, which lead to the long-term membrane stability.<sup>36,37</sup> In the before reported works, the durability of CeO<sub>2</sub>-incorporated PEMs is mainly influenced by the removal of CeO<sub>2</sub> from the PEM, which could decay the radical scavenging behavior.<sup>32</sup> To resolve it, in current work, CeO<sub>2</sub> was synthesized over ATiO<sub>2</sub> nanorods and was stable even under harsh PEMFC operating conditions, ensuring the improved chemical durability of the composite membrane than the pristine membrane. However, compared to Nafion 115 membrane, the SPEEK/CeO<sub>2</sub>-ATiO<sub>2</sub> membrane exhibited slightly a higher OCV decay.

## 5.8 | Post-durability studies

To study the impacts of the durability test, the SEM images of MEAs containing SPEEK and SPEEK/CeO<sub>2</sub>-ATiO<sub>2</sub> membranes were obtained after the durability test.

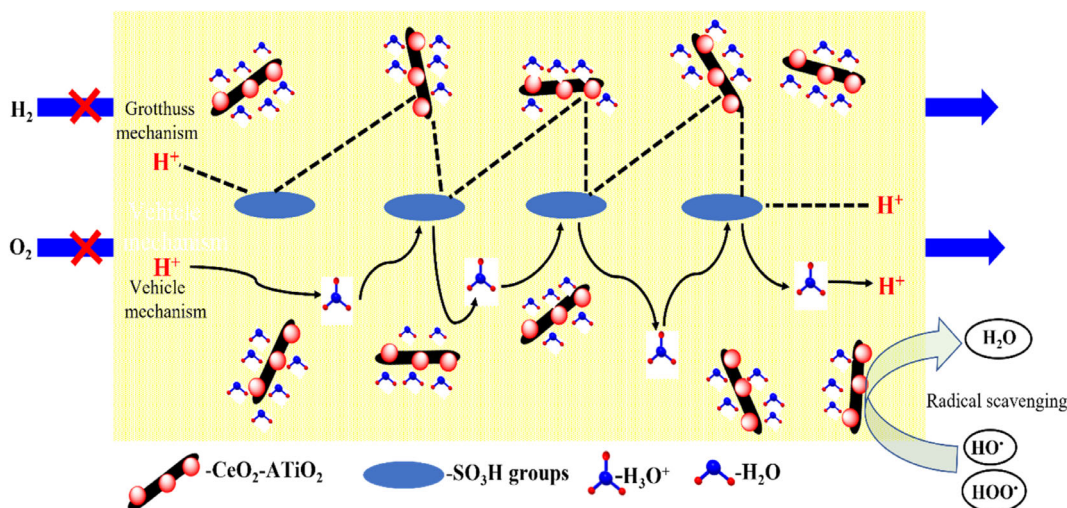
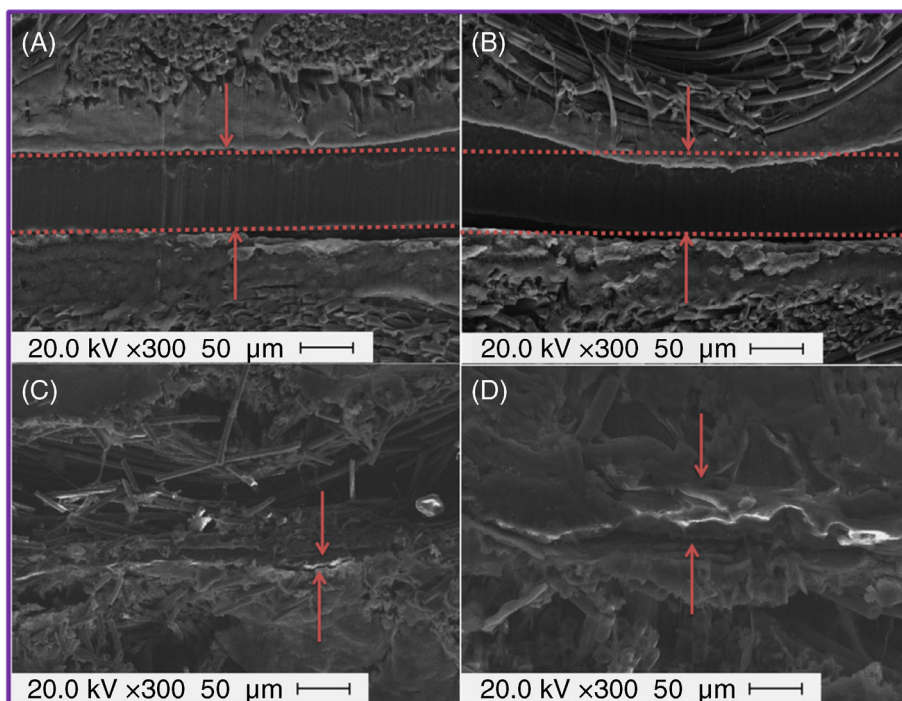


FIGURE 10 Schematic illustration of proposed proton transport mechanisms, fuel impermeability, and radical scavenging activity of SPEEK/CeO<sub>2</sub>-ATiO<sub>2</sub> hybrid membrane. SPEEK, sulfonated poly(ether ether ketone)

**FIGURE 11** Scanning electron microscopic images of MEAs before and after durability (A) and (C) SPEEK and (B) and (D) SPEEK/CeO<sub>2</sub>-ATiO<sub>2</sub>. MEA, membrane electrode assembly; SPEEK, sulfonated poly(ether ether ketone)



As displayed in Figure 11, the thickness of SPEEK was drastically lowered and membrane damaged due to the mechanical compression and radicals attack triggered by the harsh PEMFC operation. On the other hand, the SPEEK/CeO<sub>2</sub>-ATiO<sub>2</sub> (2%) nanocomposite membrane maintained most of its thickness even after the durability test that indicates high mechanical integrity and radical scavenging activity of the incorporated CeO<sub>2</sub>-ATiO<sub>2</sub> nanofiller.

## 6 | CONCLUSIONS

SPEEK/CeO<sub>2</sub>-ATiO<sub>2</sub> composite membranes with various weight percentages of CeO<sub>2</sub>-ATiO<sub>2</sub> were successfully fabricated via a solution casting method. The incorporation of CeO<sub>2</sub>-ATiO<sub>2</sub> nanofiller into the SPEEK matrix resulted in electrostatic interactions between the polymer matrixes and nanofiller that prevented the swelling of the membrane when hydrated. NH<sub>2</sub> functional groups of CeO<sub>2</sub>-ATiO<sub>2</sub> acted as an additional proton-conducting pathway via the water-free proton transfer. Thus, resulted in enhanced PEMFC performance in terms of the power density and current density of the SPEEK/CeO<sub>2</sub>-ATiO<sub>2</sub> (2%) membrane at 60°C under 100% RH and 30% RH. Furthermore, the formation of hydrogen bonding and strong electrostatic relations between the membrane backbone and nanofiller improved thermal stability and thermomechanical strength compared to the unfilled membrane. The radical scavenging property of CeO<sub>2</sub>-

ATiO<sub>2</sub> nanoparticles provided good oxidative stability and longer chemical sustainability for the SPEEK/CeO<sub>2</sub>-ATiO<sub>2</sub> (2%) membrane under acidic PEMFC conditions than the bare SPEEK membrane. It also confirmed that the development of CeO<sub>2</sub> nanoparticles on ATiO<sub>2</sub> nanorods prevented CeO<sub>2</sub> leaching, conferring the resulting membrane with prolonged radical scavenging ability. These characteristics of SPEEK/CeO<sub>2</sub>-ATiO<sub>2</sub> membranes address many of the shortcomings of SPEEK-based membranes such as low electrochemical, mechanical, and thermochemical properties. Thus, the prepared composite membrane could be the most suitable candidate for PEMFC applications under low RH condition, which may avoid the expenses of installing an external humidifier and exploitation of commercial Nafion membrane.

## CONFLICT OF INTEREST

The authors declare that they have no known competing financial interests or personal relationships that could have appeared to influence the work reported in this paper.

## ORCID

*Hariprasad Ranganathan*  <https://orcid.org/0000-0001-6797-043X>

*Mohanraj Vinothkannan*  <https://orcid.org/0000-0002-3286-9435>

*Dong Jin Yoo*  <https://orcid.org/0000-0002-5707-3361>

## REFERENCES

1. Wang Y, Chen K, Mishler J, Cho S, Adroher X. A review of polymer electrolyte membrane fuel cells: technology, applications, and needs on fundamental research. *Appl Energy*. 2011; 88(4):981-1007.
2. Singh R, Gautam A, Rai V. Graphene-based bipolar plates for polymer electrolyte membrane fuel cells. *Front Mater Sci*. 2019; 13(3):217-241.
3. Wilberforce T, El-Hassan Z, Khatib F, et al. Developments of electric cars and fuel cell hydrogen electric cars. *Int J Hydrogen Energy*. 2017;42:25695-25734.
4. Wang J, Yang B, Zeng C, et al. Recent advances and summarization of fault diagnosis techniques for proton exchange membrane fuel cell systems: a critical overview. *J Power Sources*. 2021;500:229932.
5. Wee J. Applications of proton exchange membrane fuel cell systems. *Renew Sustain Energy Rev*. 2007;11:1720-1738.
6. Kallem P, Yanar N, Choi H. Nanofiber-based proton exchange membranes: development of aligned electrospun nanofibers for polymer electrolyte fuel cell applications. *ACS Sustain Chem Eng*. 2018;7:1808-1825.
7. Pollet B, Staffell I, Shang J. Current status of hybrid, battery and fuel cell electric vehicles: from electrochemistry to market prospects. *Electrochim Acta*. 2012;84:235-249.
8. Cindrella L, Kannan A, Lin J, et al. Gas diffusion layer for proton exchange membrane fuel cells—a review. *J Power Sources*. 2009;194(1):146-160.
9. Toghyani S, Moradi NF, Afshari E, Hasanpour K, Baniyasi E, Atyabi S. Thermal and electrochemical performance analysis of a proton exchange membrane fuel cell under assembly pressure on gas diffusion layer. *Int J Hydrogen Energy*. 2018;43(9):4534-4545.
10. Chang Y, Qin Y, Yin Y, Zhang J, Li X. Humidification strategy for polymer electrolyte membrane fuel cells—a review. *Appl Energy*. 2018;230:643-662.
11. Ijaodola O, El-Hassan Z, Ogungbemi E, et al. Energy efficiency improvements by investigating the water flooding management on proton exchange membrane fuel cell (PEMFC). *Energy*. 2019;179:246-267.
12. Tüber K, Pócza D, Hebling C. Visualization of water buildup in the cathode of a transparent PEM fuel cell. *J Power Sources*. 2003;124(2):403-414.
13. Peighambaroust S, Rowshanzamir S, Amjadi M. Review of the proton exchange membranes for fuel cell applications. *Int J Hydrogen Energy*. 2010;35(17):9349-9384.
14. Escorihuela J, Narducci R, Compañ V, Costantino F. Proton conductivity of composite polyelectrolyte membranes with metal-organic frameworks for fuel cell applications. *Adv Mater Interfaces*. 2018;6:1801146.
15. Houchins C, Kleen G, Spendelow J, et al. US DOE progress towards developing low-cost, high performance, durable polymer electrolyte membranes for fuel cell applications. *Membranes*. 2012;2(4):855-878.
16. Yee R, Rozendal R, Zhang K, Ladewig B. Cost effective cation exchange membranes: a review. *Chem Eng Res Des*. 2012;90(7): 950-959.
17. Xie Q, Li Y, Chen X, Hu J, Li L, Li H. Composite proton exchange membranes based on phosphosilicate sol and sulfonated poly(ether ether ketone) for fuel cell applications. *J Power Sources*. 2015;282:489-497.
18. Gao S, Xu H, Fang Z, et al. Highly sulfonated poly(ether ether ketone) grafted on graphene oxide as nanohybrid proton exchange membrane applied in fuel cells. *Electrochim Acta*. 2018;283:428-437.
19. Lei M, Hamel C, Chen K, et al. Thermomechanical behaviors of polyether ether ketone (peek) with stretch-induced anisotropy. *J Mech Phys Solids*. 2021;148:104271.
20. Chang J, Park J, Park G, Kim C, Park O. Proton-conducting composite membranes derived from sulfonated hydrocarbon and inorganic materials. *J Power Sources*. 2003;124(1):18-25.
21. Rambabu G, Bhat S. Simultaneous tuning of methanol cross-over and ionic conductivity of SPEEK membrane electrolyte by incorporation of PSSA functionalized MWCNTs: a comparative study in DMFCs. *Chem Eng J*. 2014;243:517-525.
22. Xing P, Robertson G, Guiver M, Mikhailenko S, Wang K, Kaliaguine S. Synthesis and characterization of sulfonated poly(ether ether ketone) for proton exchange membranes. *J Membr Sci*. 2004;229(1-2):95-106.
23. Bose S, Kuila T, Nguyen T, Kim N, Lau K, Lee J. Polymer membranes for high temperature proton exchange membrane fuel cell: recent advances and challenges. *Prog Polym Sci*. 2011; 36(6):813-843.
24. Zhang H, Shen P. Recent development of polymer electrolyte membranes for fuel cells. *Chem Rev*. 2012;112(5):2780-2832.
25. Li Y, Zhang M, Wang X, Li Z, Zhao L. Anhydrous conducting composite membranes composed of SPEEK/silica/ionic liquids for high-temperature proton exchange. *Electrochim Acta*. 2016; 222:1308-1315.
26. Kim A, Gabunada J, Yoo D. Amelioration in physicochemical properties and single cell performance of sulfonated poly(ether ether ketone) block copolymer composite membrane using sulfonated carbon nanotubes for intermediate humidity fuel cells. *Int J Energy Res*. 2019;43(7):2974-2989.
27. Jiang Z, Zhao X, Manthiram A. Sulfonated poly(ether ether ketone) membranes with sulfonated graphene oxide fillers for direct methanol fuel cells. *Int J Hydrogen Energy*. 2013;38(14): 5875-5884.
28. Kim A, Vinothkannan M, Song M, Lee J, Lee H, Yoo D. Amine functionalized carbon nanotube (ACNT) filled in sulfonated poly(ether ether ketone) membrane: effects of ACNT in improving polymer electrolyte fuel cell performance under reduced relative humidity. *Compos Part B Eng*. 2020;188:107890.
29. Ghosh P, Dhole C, Ganguly S, Banerjee D, Kargupta K. Phosphosilicate gel-sulfonated poly(ether ether ketone) nanocomposite membrane for polymer electrolyte membrane fuel cell. *Mater Today Proc*. 2018;5(1):2186-2192.
30. Fu Y, Manthiram A, Guiver M. Blend membranes based on sulfonated poly(ether ether ketone) and polysulfone bearing benzimidazole side groups for proton exchange membrane fuel cells. *Electrochem Commun*. 2006;8(8):1386-1390.
31. Salarizadeh P, Javanbakht M, Pourmahdian S. Enhancing the performance of SPEEK polymer electrolyte membranes using functionalized TiO<sub>2</sub> nanoparticles with proton hopping sites. *RSC Adv*. 2017;7(14):8303-8313.
32. Parnian MJ, Rowshanzamir S, Prasad AK, Advani SG. Effect of ceria loading on performance and durability of sulfonated poly(ether ether ketone) nanocomposite membranes for proton exchange membrane fuel cell applications. *J Membr Sci*. 2018; 565:342-357.



33. Liu X, Zhang Y, Deng S, et al. Semi-interpenetrating polymer network membranes from SPEEK and BPPO for high concentration DMFC. *ACS Appl Energy Mater.* 2018;1(10):5463-5473.
34. Kim A, Vinothkannan M, Lee K, et al. Ameliorated performance of sulfonated poly(arylene ether sulfone) block copolymers with increased hydrophilic oligomer ratio in proton-exchange membrane fuel cells operating at 80% relative humidity. *Polymers.* 2020;12(9):1871.
35. Hariprasad R, Vinothkannan M, Kim AR, Yoo DJ. SPVdF-HFP/SGO nanohybrid proton exchange membrane for the applications of direct methanol fuel cells. *J Dispers Sci Technol.* 2019;42(1):33-45.
36. Vinothkannan M, Ramakrishnan S, Kim AR, Lee HK, Yoo DJ. Ceria stabilized by titanium carbide as a sustainable filler in the Nafion matrix improves the mechanical integrity, electrochemical durability, and hydrogen impermeability of proton-exchange membrane fuel cells: effects of the filler content. *ACS Appl Mater Interfaces.* 2020;12(5):5704-5716.
37. Vinothkannan M, Hariprasad R, Ramakrishnan S, Kim AR, Yoo DJ. Potential bifunctional filler (CeO<sub>2</sub>-ACNTs) for Nafion matrix toward extended electrochemical power density and durability in proton-exchange membrane fuel cells operating at reduced relative humidity. *ACS Sustain Chem Eng.* 2019;7(15):12847-12857.
38. Salarizadeh P, Javanbakht M, Pourmahdian S, Beydaghi H. Influence of amine-functionalized iron titanate as filler for improving conductivity and electrochemical properties of SPEEK nanocomposite membranes. *Chem Eng J.* 2016;299:320-331.
39. Ketpang K, Lee K, Shanmugam S. Facile synthesis of porous metal oxide nanotubes and modified Nafion composite membranes for polymer electrolyte fuel cells operated under low relative humidity. *ACS Appl Mater Interfaces.* 2014;6(19):16734-16744.
40. Shengnan Z, Firas A, Natalie J, David RM, Andrew JR. A comparison of the strength of autohesion of plasma treated amorphous and semi-crystalline PEEK films. *Polym Adv Technol.* 2011;22(12):2496-2502.
41. Huang RYM, Pinghai SC, Burns M, Feng X. Sulfonation of poly(ether ether ketone)(PEEK): kinetic study and characterization. *J Appl Polym Sci.* 2001;82(11):2651-2660.
42. Hong W, Xiaohui S, Tao X, Weiqiang H, Zhongyi J. Sulfonated poly(ether ether ketone)/amino-acid functionalized titania hybrid proton conductive membranes. *J Power Sources.* 2012;213:83-92.
43. Sowmya G, Gowrishankar S, Ramesh PM. Influence of phosphotungstic acid in sulfonated poly (ether ether ketone)/poly (amide imide) based proton conductive membranes and its impact on the electrochemical studies of microbial fuel cell application. *Ionics.* 2020;26:1841-1852.
44. Myles T, Bonville L, Maric R. Catalyst, membrane, free electrolyte challenges, and pathways to resolutions in high temperature polymer electrolyte membrane fuel cells. *Catalysts.* 2017;1:16.
45. Muhammad AI, Tiantian L, Xuemei W, Xiaoming Y, Abdul SK, Gaohong H. Sulfonated polybenzimidazole/amine functionalized titanium dioxide (sPBI/AFT) composite electrolyte membranes for high temperature proton exchange membrane fuel cells usage. *Chin J Chem Eng.* 2020;28(9):2425-2437.
46. Myungseong H, Yong GS, Hyejin L, Dongwon S, Byungchan B. Accelerated testing of polymer electrolyte membranes under open-circuit voltage conditions for durable proton exchange membrane fuel cells. *Int J Hydrog Energy.* 2017;52(42):30787-30791.
47. Jinfeng W, Xiao ZY, Jonathan JM, et al. A review of PEM fuel cell durability: degradation mechanisms and mitigation strategies. *J Power Sources.* 2008;184:104-119.
48. Vishal M, Russell K, James F. H<sub>2</sub>O<sub>2</sub> formation mechanism in PEMFC. *ECS Trans.* 2006;1(8):295-301.
49. Lei Z, Sanjeev M. Investigation of durability issues of selected nonfluorinated proton exchange membranes for fuel cell application. *J Electrochem Soc.* 2006;153:A1062.
50. Hongying H, Maria LDV, Philippe K. Durability of sulfonated aromatic polymers for proton-exchange-membrane fuel cells. *ChemSusChem.* 2011;4(11):1526-1536.

## SUPPORTING INFORMATION

Additional supporting information may be found in the online version of the article at the publisher's website.

**How to cite this article:** Ranganathan H, Vinothkannan M, Kim AR, Subramanian V, Oh M-S, Yoo DJ. Simultaneous improvement of power density and durability of sulfonated poly (ether ether ketone) membrane by embedding CeO<sub>2</sub>-ATiO<sub>2</sub>: A comprehensive study in low humidity proton exchange membrane fuel cells. *Int J Energy Res.* 2022;46(7):9041-9057. doi:10.1002/er.7781